Biomaterials 35 (2014) 6954–6963

Contents lists available at ScienceDirect

Biomaterials

journal homepage: www.elsevier.com/locate/biomaterials

The effect of fibrillar matrix architecture on tumor cell invasion of physically challenging environments

Asja Guzman, Michelle J. Ziperstein, Laura J. Kaufman*

Department of Chemistry, Columbia University, New York, NY 10027, USA

ARTICLE INFO

Article history:
Received 18 February 2014
Accepted 18 April 2014
Available online 15 May 2014

Keywords:
Collagen
Breast cancer
Cell invasion
3D
Extracellular matrix

ABSTRACT

Local invasion by and dissemination of cancer cells from a primary tumor are key initial steps of metastasis, the most lethal aspect of cancer. To study these processes *in vitro*, the invasion of cells from multicellular breast cancer aggregates embedded in three-dimensional (3D) extracellular matrix culture systems was studied. This work showed that in 3D fibrillar environments composed of collagen I, pore size – not the viscoelastic properties of the matrix – was the biophysical characteristic controlling breast cancer cell invasion efficiency. Furthermore, it was shown that fibrillar matrix architecture is a crucial factor that allows for efficient 3D invasion. In a 3D non-fibrillar environment composed of basement membrane extract (BME), invasion efficiency was greatly diminished, the mesenchymal individual mode of 3D invasion was abolished, and establishment of cell polarity and protrusions was compromised. These effects were seen even though the BME matrix has invasion permissive viscoelasticity and suitable adhesion ligands. The altered and limited invasive behavior observed in BME was rescued through introduction of fibrillar collagen into the non-fibrillar matrix. The biophysical cues of fibrillar collagen facilitated efficient invasion of sterically disadvantageous environments through assisting cell polarization and formation of stable cell protrusions. Finally, we suggest the composite matrices employed in this study consisting of fibrillar collagen I and BME in either a liquid-like or gelled state are suitable for a wide range of 3D cell studies, as these matrices combine fibrillar features that require cells to deploy integrin-dependent mechanotransduction machinery and a tunable non-fibrillar component that may require cells to adopt alternative migratory modes.

1. Introduction

Extracellular matrix (ECM) is a complex mixture of structural macromolecules and cytokines that regulates key cellular processes including polarization, differentiation, and proliferation through biochemical and biophysical cues. Altered ECM properties have been associated with numerous pathological conditions including atherosclerosis [1], fibrotic diseases [2–4], and cancer [5,6]. In all cases, changes to the ECM are not simply symptoms of disease but are contributors to the pathogenic process.

In cancer, alterations in ECM composition and organization have been implicated in the progression of malignant tumors from circumscribed masses to locally invading entities to eventual metastatic disease. While cancer progression is regulated by a complex interplay of genetic and epigenetic changes, evolving interactions between tumor cells and the surrounding ECM play a critical role in the metastatic cascade [7,8].

The importance of the local environment and changes to that environment have attracted particular attention among breast cancer researchers, as high breast tissue density has been associated with both higher risk of breast cancer and poor prognosis in patients [9,10]. High breast tissue density is due to higher than average amounts of the fibrillar structural protein collagen I, and elevated amounts of this protein – as well as fibrillar collagen III – in and around tumors have been demonstrated by both histology and genetic profiling [11–15].

ECM surrounding breast tumors differs not only in biochemical composition from that of normal tissue but also in physical properties, notably stiffness [16]. A recent study correlated the stiffness of and around breast tumors with their aggressiveness [17]. The effect of stiffness on cell spreading and migratory capacity has been well studied on two dimensional (2D) substrates [18,19]. Such studies have also been undertaken in more physiologically relevant three-dimensional (3D) environments, though isolating effects of stiffness from those of ligand availability and network architecture is a significant challenge in the 3D context [20–24].

* Corresponding author.
E-mail address: kaufman@chem.columbia.edu (L.J. Kaufman).

http://dx.doi.org/10.1016/j.biomaterials.2014.04.086
0142-9612/

Beyond differences in composition and stiffness, the ECM surrounding invasive breast tumors also demonstrates changes in network architecture relative to normal ECM. Increased deposition of fibrillar collagens may lead to decreased porosity near the tumor. Moreover, cellular remodeling of fibrillar collagens may lead to heterogeneities in density and network organization. Indeed, architectural changes in ECM have been correlated with breast cancer prognosis. Alignment and orientation of collagen I fibers perpendicular to the tumor boundary has been associated with recurrence after surgical excision and metastasis, and breast cancer cells have been shown to migrate preferentially along radially aligned collagen fibers at the interface of the primary tumor and ECM [25,26].

In sum, accumulating evidence suggests that the presence and particular organization of fibrillar collagen I is a marker of and/or a causal factor in breast cancer invasion. Here, we dissect the contributions of biophysical properties of fibrillar collagen I to the invasion efficiency of breast cancer cells. In particular, the invasion of triple negative highly aggressive breast adenocarcinoma cells (MDA-MB-231) cultured as multicellular tumor spheroids (MTSs) in both 3D (cells immersed within a matrix) and pseudo-3D (cells placed atop a thick matrix) settings was studied. The multicellular invasion efficiency as reflected by invasive distance was analyzed. Invasive mode as reflected by cell polarization, establishment of protrusions, and ECM rearrangement on both the spheroid and single cell level was also investigated. The 3D matrices employed were composed of either fibrillar collagen I and/or non-fibrillar basement membrane extract (BME). The matrices were prepared so as to exhibit stiffnesses that varied over two orders of magnitude and displayed distinct network architectures, with varying porosity and fibrillar dimensions.

2. Materials and methods

2.1. Cell lines and reagents

MDA-MB-231 breast cancer cells were obtained from the American Type Culture Collection (Manassas, VA). All cell culture reagents unless otherwise stated were obtained from Gibco (Grand Island, NY). Acid-solubilized (AS) rat tail collagen I was obtained from BD Biosciences (San Jose, CA) as an 8.5–9 mg/ml solution. Pepsin-treated (PT) bovine collagen I was obtained from Advanced BioMatrix (San Diego, CA) as a 5.9–6.1 mg/ml solution. Growth factor-reduced, phenol red-free basement membrane extract (BME)/Matrigel was obtained as an 8.9–9.4 mg/ml solution from BD Biosciences (San Jose, CA). 10× DMEM solution, sterile NaOH (1 N), and sodium bicarbonate solution (7.5%) were purchased from Sigma Aldrich (St. Louis, MO). Gibco 4-(2-hydroxyethyl)-1-piperazineethanesulfonic acid (HEPES) buffer (1 M) was obtained from Invitrogen (Carlsbad, CA). Aprotinin, leupeptin, pepstatin A, and E-64 were obtained from MP Biomedicals (Solon, OH). Triton-X, marimastat (BB-2516), and blebbistatin were obtained from EMD Millipore Chemicals (Billerica, MA). Alexa Fluor-conjugated phalloidin was obtained from Invitrogen Life Technologies (Grand Island, NY), and 1.0 mg/ml propidium iodide solution was obtained from Sigma Aldrich. 10% buffered formalin phosphate, acetone, and ethanol were obtained from Fisher Scientific (Pittsburgh, PA).

2.2. Cell culture and generation of multicellular tumor spheroids

Cells were cultured in growth medium consisting of 1× high glucose DMEM containing 10% (v/v) FBS, 1% (v/v) 100× penicillin/streptomycin solution, and 1% (v/v) 100× non-essential amino acids solution at 37 °C with 5% carbon dioxide. Cells were subcultured when 70–80% confluent. Multicellular tumor spheroids (MTSs) were formed using the Perfecta 3D Biomatrix hanging drop system (Neta Scientific, Hainesport, NJ). 30 μl drops of a 4×10^5 cells/ml cell suspension were placed in the wells of the hanging drop plate. Droplets were held in place by surface tension, and cells accumulated at the bottom of each droplet to form a spheroid, or MTS. Spheroids were allowed to form and grow for 6 days at 37 °C with 5% carbon dioxide.

2.3. Cell treatments

Blebbistatin was used to inhibit myosin II-phosphorylation and was added to the growth medium at 10–20 μM in 2D experiments. When blebbistatin was used for cells embedded in 3D matrices, the drug concentration in the overlaying medium was increased to achieve a 20 μM concentration within the 3D gel. Thus, 200 μl gels were overlaid with 50 μl of 100 μM blebbistatin containing growth medium. DMSO was used as the solvent control at equivalent concentrations. Inhibition of endogenous proteases for cells cultured in 3D environments was achieved through addition of a protease inhibitor cocktail as described in Wolf et al. [27]. Both the collagen solution and the growth medium added on top of the 3D collagen matrix were supplemented with 100 μM marimastat, 250 μM E-64, 100 μM pepstatin A, 2 μM leupeptin, and 2.2 μM aprotinin.

2.4. Preparation of cell free gels

Collagen gel solutions from 1.0 to 4.0 mg/ml were prepared by diluting the high-concentration collagen stock solutions. Appropriate amounts of collagen stock solution were prepared with 10% (v/v) 10× DMEM, 2.5% (v/v) HEPES buffer, 2.5% (v/v) sodium bicarbonate and distilled, deionized water. To prevent self-assembly of collagen monomers, all solutions were held and mixed at 4 °C. NaOH was added to adjust the pH to 7.4, and the gel was transferred immediately to the chosen gelation temperature (22 °C or 37 °C). Collagen solutions were allowed to gel for 45 min, which was sufficient to complete gelation at either temperature, and then transferred to the incubator at 37 °C.

BME gels were prepared by diluting the BME stock solution (8.9–9.4 mg/ml) with ice-cold 1× DMEM (serum free) to the required concentration. All steps were performed at 4 °C with pre-chilled solutions and instruments. Solutions were transferred immediately to an incubator at 37 °C and allowed to gel for 45 min.

To prepare collagen/BME composite gels, first 10× DMEM, HEPES buffer, and sodium bicarbonate were mixed. Then, the required amount of BME stock solution was added. This solution replaced a proportion of the H_2O that would be added in the equivalent pure collagen gel. Subsequently the collagen stock solution was added and the solution was brought to pH 7.4 by adding NaOH. After careful mixing, the solution was transferred to the chamber and gelled at 37 °C.

2.5. Preparation of cell-embedded gels

To prepare collagen gels loaded with a single MTS, collagen solution was prepared as described above. 200 μl of neutralized collagen solution was added to a chamber consisting of a 5 mm glass cylinder glued to a coverslip-bottom cell culture dish. A nylon mesh was placed on the inner circumference of the cylinder to anchor the collagen gel. The spheroid was added to the liquid collagen in 7 μl growth medium. The chamber was then transferred immediately to the desired temperature for gelation (45 min) and then to the 37 °C incubator. The collagen gels were overlaid with 40–50 μl growth medium after 2 h and surrounded by additional liquid to prevent drying during extended incubation periods. To prepare BME and collagen/BME composite matrices loaded with a single MTS, the chambers were first pre-coated with BME or a collagen/BME solution to prevent sedimentation of MTSs to the bottom of the chamber. The coating was gelled at 37 °C. Following this, the bulk volume of the matrix solution was added to the chamber and individual spheroids implanted as described above.

To prepare collagen gels loaded with dispersed cells, the collagen solution was prepared omitting the water and was neutralized at 4 °C. The water was substituted with ice-cold growth medium containing the desired number of cells. Subsequently 70–200 μl of cell-loaded collagen was added to the chamber and gelled at 22 °C or 37 °C as described above for MTS loaded collagen gels. After 2 h gels were overlaid with 40–50 μl growth medium. For preparation of BME gels with dispersed cells, part of the DMEM was substituted with medium containing the desired number of cells. After careful mixing of the cell-containing liquid component with the BME, the solution was added to the chamber and transferred to the 37 °C incubator. After 2 h gels were overlaid with 40–50 μl growth medium. To prepare cell-embedded composite matrices, the mixture was prepared omitting H_2O and substituted with cells suspended in serum-free medium that was added after the collagen/BME solution was brought to physiological pH. Gelling and overlay were performed as described for the BME gels.

2.6. Collagen contraction assay

Collagen solutions of different collagen concentration containing 5×10^5 MDA-MB-231 cells/ml were prepared, and 500 μl gels were cast onto the 23 mm coverslip bottom of FluroDishes (35 mm). Gels were polymerized for 60 min at either 22 °C or 37 °C, overlaid with 2 ml growth medium, and manually released from the glass bottom. Contraction was allowed for 24 h at normal incubation conditions. Gel contraction was documented using digital photography. Images were taken at $t = 0$ h (before gel release) and at $t = 24$ h, and gel area was measured. Contraction is expressed as a percentage decrease of gel area over 24 h. All conditions were tested in triplicate.

2.7. Immunocytochemistry

For immunocytochemical staining, dispersed cells were embedded in or plated on matrices of 100–200 μl. Cells were fixed in neutrally buffered 4% formalin solution for 20 min at 24 °C. After extensive washing and permeabilization with 0.5% Triton-X, samples were washed again with PBS to remove the detergent, fluorescently labeled phalloidin was added and the samples were incubated for 16–24 h at 4 °C. After extensive washing with PBS, samples were overlaid with PBS and immediately subjected to imaging.

2.8. Transwell migration assay

MDA-MB-231 cells were detached with Accutase cell detachment solution from EMD Millipore Chemicals (Billerica, MA) and re-suspended in DMEM containing 2% (v/v) FBS, 1% (v/v) 100× penicillin/streptomycin solution and the respective drugs to a concentration of 3.75×10^5 cells/ml. 200 μl of cell suspension was plated into the FluoroBlok Transwell insert (BD Biosciences, San Jose, CA) and placed into a well of a 24-well cell culture plate supplemented with 500 μl of DMEM containing 10% (v/v) FBS, 1% (v/v) 100× penicillin/streptomycin solution, and the respective drugs. Cells were allowed to migrate for 24 h at normal incubation conditions. Cells were then fixed with −20 °C acetone, stained with 0.01% (v/v) propidium iodide for 1 h at 37 °C and washed with PBS. Membranes were excised from the Transwell inserts, mounted in Vectashield mounting medium (Vector Laboratories, Burlingame, CA) and imaged with an epi-fluorescence microscope. For quantification 20 images were taken from each sample.

2.9. Microscopy and image analysis

Spheroids and individual cells in 3D matrices were imaged with a 10× (NA = 0.4) air or 60× (NA = 1.42) oil objective on the inverted confocal laser-scanning microscope (Olympus Fluoview 300) in scanning transmittance, confocal fluorescence, or confocal reflectance mode. An Argon ion laser at 488 nm was used for excitation unless otherwise specified and a photo-multiplier tube (PMT) for detection. Live cell imaging was performed using a custom-built microscope incubation chamber and objective heater to keep cells at 37 °C at 5% CO_2. At least four spheroids in each type of gel were imaged at 2 h and 24 h after implantation, with the particular number of spheroids assessed noted in the figure captions. From the 10× spheroid images, invasive distance – defined as the difference between the periphery of the spheroid at $t = 2$ h and a circle that circumscribed 90% of the invasive cells at $t = 24$ h – was determined for each spheroid.

For visualization of the actin cytoskeleton and analysis of cell morphology and protrusions, confocal fluorescent images of fixed cells stained with fluorescently labeled phalloidin were acquired with the 60× objective. For imaging cells plated atop matrices (pseudo-3D), the limited working distance of the objective required that the gels be removed from the cell/gel chambers and be placed upside down on a coverslip, while this procedure was not required for cells dispersed in the matrix. In all cases, a 543 nm HeNe laser was used for excitation, and detection was performed through a longpass 570 nm filter. Maximum intensity projections from z-stacks of 10–20 μm (step size 2.5 μm) were generated using a home-written Matlab script.

Collagen was imaged via confocal reflectance microscopy (CRM) with the 60× oil objective using the 488 nm laser for excitation and a PMT for detection. Pore size analysis was performed on collagen images as described previously [28].

2.10. Rheology

Rheological experiments were conducted on an Anton Paar MCR 302 with a modified glass bottom and built-in Peltier temperature control. A ~1° polycarbonate cone geometry with evaporation blocker was used. In all cases, 750 μl of neutralized collagen, BME, or collagen/BME solution was applied to the measuring stage at 37 °C or 22 °C. The sample was allowed to gel for 10–30 min depending on the gel type. Measurements were then performed in oscillatory mode at $\omega = 1$ Hz and $\gamma = 0.8\%$, within the linear viscoelastic regime. Storage modulus G′ (Pa) and loss modulus G″ (Pa) were measured every 30 s for 10 min, and all tests were repeated 2–3 times.

3. Results

To establish the range of ECM composition, mechanical properties, and network architectures that support multicellular spheroid invasion of triple negative breast adenocarcinoma (MDA-MB-231) cells, we studied MTS invasion in fibrillar (collagen I), non-fibrillar (BME), and composite matrices in both true 3D (cells immersed within the matrix) and pseudo-3D scenarios (cells placed atop a thick matrix) (Fig. 1a and b).

3.1. Impact of physical matrix characteristics on 3D spheroid invasion

The impact of collagen concentration on MTS invasion in fibrillar pseudo-3D and true 3D settings over 24 h was assessed using

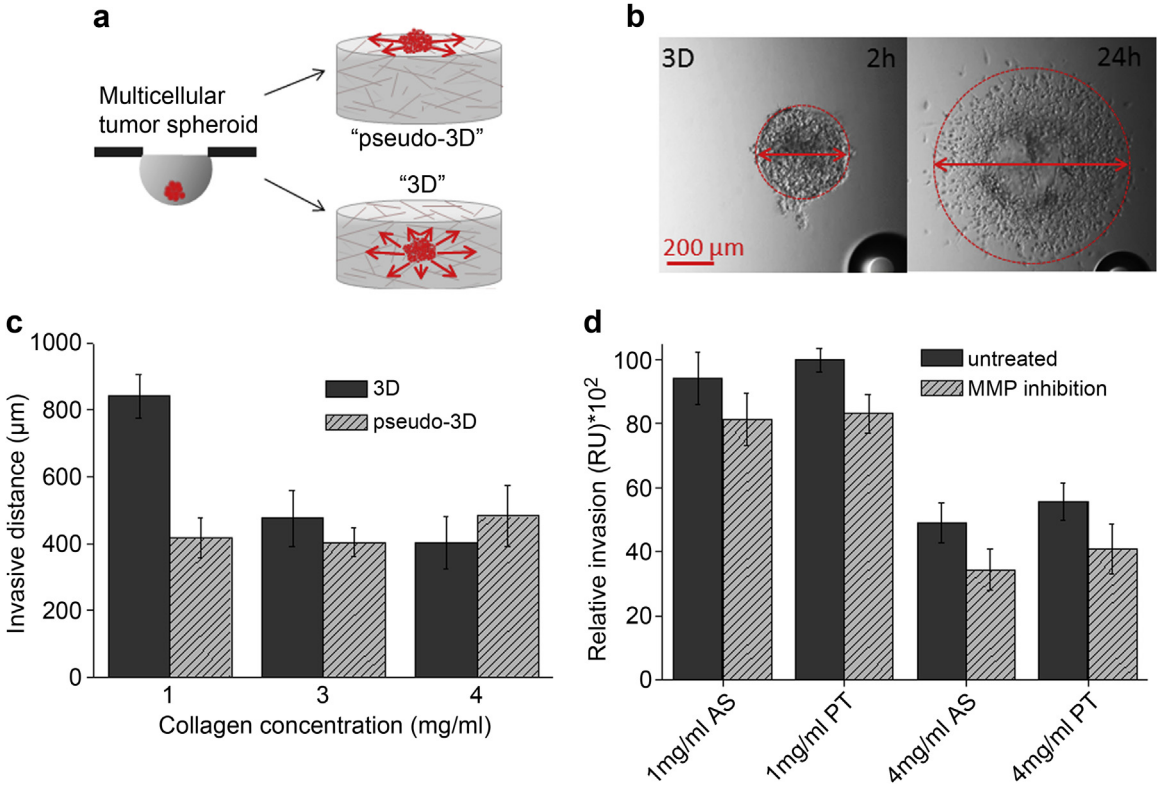

Fig. 1. MDA-MB-231 MTS invasion in 3D collagen matrices with different collagen concentrations. (*a*) Experimental setup for invasion analysis of an MTS atop ("pseudo-3D") and within ("3D") biopolymer gels. (*b*) Transmitted light images of a representative MTS implanted in a collagen gel at 2 h and 24 h after implantation. Red line depicts the diameter of the MTS before and after invasion, and invasive distance is defined as the difference between these diameters. Scale bar = 200 μm. (*c*) MTS invasion at $t = 24$ h in 3D (solid) and pseudo-3D (shaded) PT collagen gels. Mean values ± SD are shown, sample number $n > 15$ for every 3D condition, $n \geq 5$ for every pseudo-3D condition. (*d*) Comparison of MTS invasion at $t = 24$ h in 3D AS and PT collagen without (solid) and with (shaded) protease inhibition. Relative mean values normalized to the 1.0 mg/ml PT untreated control ± SD are shown. $n = 6$–10 for every condition (For interpretation of the references to color in this figure legend, the reader is referred to the web version of this article.).

pepsin-treated (PT) collagen to generate the matrices. In pseudo-3D, the invasion showed no statistically significant dependence on collagen density. In contrast, for MTSs embedded in these environments, where the full 3D architecture of the network plays a role, a clear decrease of invasion with increasing collagen concentration was seen (Fig. 1c). We suggest that the physical constraints of the system imposed by the increased number of collagen fibers and resulting dense meshwork limit the invasive behavior.

To dissect the contributions of stiffness and various aspects of network architecture to MTS invasion efficiency, invasion in a tunable acid-solubilized (AS) collagen system was investigated. First, we established that invasion as a function of collagen concentration in 3D AS collagen gelled at 37 °C mirrors that in 3D PT collagen as shown in Fig. 1c. When gelled at 37 °C, 1.0 mg/ml AS collagen matrices have comparable viscoelasticity and pore size to PT collagen gels of the same concentration. Biochemically, AS collagen differs from PT collagen in that its monomers bear non-helical telopeptides that are sites for enzymatic cross-linking. We compared MDA-MB-231 MTS invasive distances and invading cell morphology in telopeptide-intact (AS) and -deficient (PT) collagen gels of 1.0 mg/ml and 4.0 mg/ml collagen with and without pharmacological protease inhibition. We found that the presence of telopeptides did not influence invasion efficiency in 3D collagen matrices at either concentration (Fig. 1d). The migratory phenotype observed was very similar in all cases: cells emerging from the spheroid were polarized and invaded individually, generally in an axial orientation relative to the spheroid. At 24 h after implantation, some cells well beyond the periphery of the spheroid demonstrated a stellate morphology bearing long filopodia while other cells were round. In both AS and PT collagen at 1.0 and 4.0 mg/ml, a mixed population of strongly polarized and round cells was evident, with no clear difference in the proportion of cells of each morphological class in these environments. Moreover, in AS and PT collagen at 1.0 and 4.0 mg/ml collagen, the effect of protease inhibition on invasive distance was limited (Fig. 1d), and no obvious morphological changes were detected in the invading cells. Given these results, AS and PT collagen matrices were considered comparable substrates for the cells, and a tunable AS collagen system was then employed to decouple the effects of stiffness and network architecture on invasion efficiency.

Matrix properties of AS collagen change substantially with gelation temperature. AS (and PT) collagen gelled at 37 °C yields a matrix of thin well-dispersed fibrils while AS collagen gelled at lower temperatures results in a matrix of highly bundled fibers (Fig. 2a) [29,30]. While such gels have larger pore size relative to a gel of the same concentration formed at physiological temperature, they also have increased stiffness since elasticity depends on both network porosity and properties of the struts constituting the fibrillar network (Fig 2a; Supplementary Table 1) [30].

Analysis of invasive distances at 24 h for MTSs embedded in each matrix type represented by Fig. 2a revealed that spheroid invasion in 3D fibrillar collagen I matrices is a robust cellular

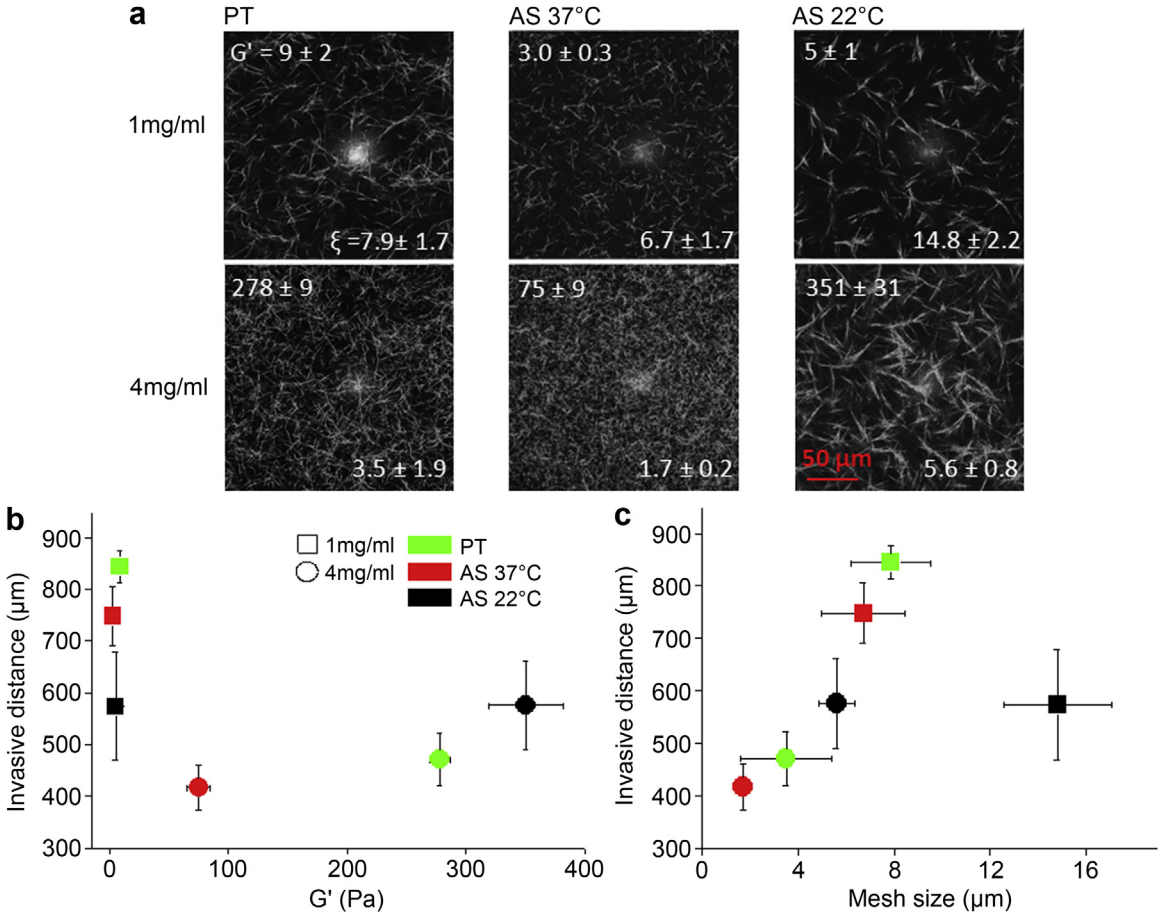

Fig. 2. Dependence of invasion on fibrillar matrix biophysical properties. (*a*) CRM images of (left) PT collagen, (middle) AS collagen gelled at 37 °C, and (right) AS collagen gelled at 22 °C at (top) 1.0 mg/ml and (bottom) 4.0 mg/ml. Bright spots visible in some CRM images are artifacts due to reflection from optical elements within the microscope and are removed prior to pore size analysis as described in Ref. [28]. Scale bar = 50 µm. Text in the upper left corner of each panel shows the storage modulus G′ (Pa) ± SD, and text in the lower right corner shows the average pore size ξ (µm) ± SD over $n \geq 5$ gels. (*b, c*) MTS 3D invasive distance as function of matrix (b) storage modulus, G′, and (c) pore size, ξ. All values are given ± SD. Error bars are not visible if smaller than symbols. Legend in (b) applies to (b) and (c).

behavior. Indeed, invasive distances at least as large as the initial spheroid diameter were measured in collagen gels with storage moduli spanning two orders of magnitude (3–350 Pa) and pore size spanning one order of magnitude (1.5–15 μm) (Fig. 2; Supplementary Table 1). Optimal invasion was observed in 1.0 mg/ml PT collagen, which is a highly compliant gel ($G' = 9$ Pa) with pore size approximating the MDA-MB-231 nuclear dimension ($\xi = 8$ μm, nucleus cross section = 6–8 μm) [31]. Inspection of invasive distance as a function of collagen concentration, elasticity of the matrix, fiber thickness, and network pore size shows that among these variables pore size is the strongest determinant for MDA-MB-231 MTS invasion efficiency in 3D fibrillar collagen systems (Fig. 2b and c). Statistical analysis via Pearson's product–moment correlation demonstrated no significant correlation between invasion and storage modulus ($r = -0.47$); indeed three matrices with very similar low G′ values exhibited a range of invasive capacity from moderate to maximal (Fig. 2b). On the other hand, the pore size of the fibrillar matrix did correlate with invasion efficiency. This correlation was biphasic, and a positive Pearson correlation between pore size and invasion for a range of pore sizes from 1.5 to 9.6 μm was seen ($r = 0.96$). Optimal pore size was ≈8 μm, and limited invasion was seen at both small pore sizes where steric constraints are expected to be important and at the largest pore size ($\xi \approx 15$ μm) where reduced substrate availability may play a role. The degree of bundling of the collagen fibers did not have a clear effect on MDA-MB-231 MTS invasion, with comparable invasion in matrices of similar pore size but different fiber thickness (Fig. 2c).

The limited invasion observed in the smallest pore size environments suggests sub-nuclear pore size is a key rate-limiting factor during 3D invasion. If this is the case, cellular players involved in cell contraction are likely to be central for efficient 3D invasion. To test this hypothesis, cell migration was analyzed under inhibition of cell contractility by blocking myosin II-phosphorylation through blebbistatin application [32,33]. Individual cells and MTSs under myosin II inhibition were subjected to transmigration assays utilizing stiff membranes of defined pore size or invasion assays in collagen I matrices with comparable pore sizes. In these assays, MDA-MB-231 cells had obvious difficulty moving through 3 μm pores even without inhibition, showing that sub-nuclear pore size can strongly inhibit invasion (Fig. 3a). Myosin II inhibition in these assays nearly abolished migration through restricting pores while reducing it ≈40% in membranes with non-restricting pores (Fig. 3a). Restricting pore size in collagen matrices had a lesser effect on MTS invasion overall, and blebbistatin treatment caused a comparable reduction of invasion distance in collagen lattices with non-restricting average pore size (8 μm) and those with subcellular sized pores (3 μm) (Fig. 3b). These findings suggested that the deformability of the pore and/or the presence of collagen fibers might assist tumor cells in invading physically constraining 3D environments.

3.2. Invasion mode and efficiency in non-fibrillar matrices

To investigate 3D invasion without the physical cues of collagen fibers, MTS invasion assays were performed on pseudo-3D and in true 3D matrices composed of basement membrane extract (BME) in various concentrations (Fig. 4). BME consists primarily of laminin and collagen IV, which form sheet-like structures providing a dense meshwork with sub-micron pores [34–36], in contrast to the relatively large pore size, fibrillar architecture of collagen I networks. While the network architecture of BME gels is distinct from that of fibrillar collagen matrices, their viscoelastic properties are similar, with the BME gels used in this study having comparable storage moduli to 1.0 mg/ml PT and AS (37 °C) collagen I matrices (Fig 4b, inset; Supplementary Table 1).

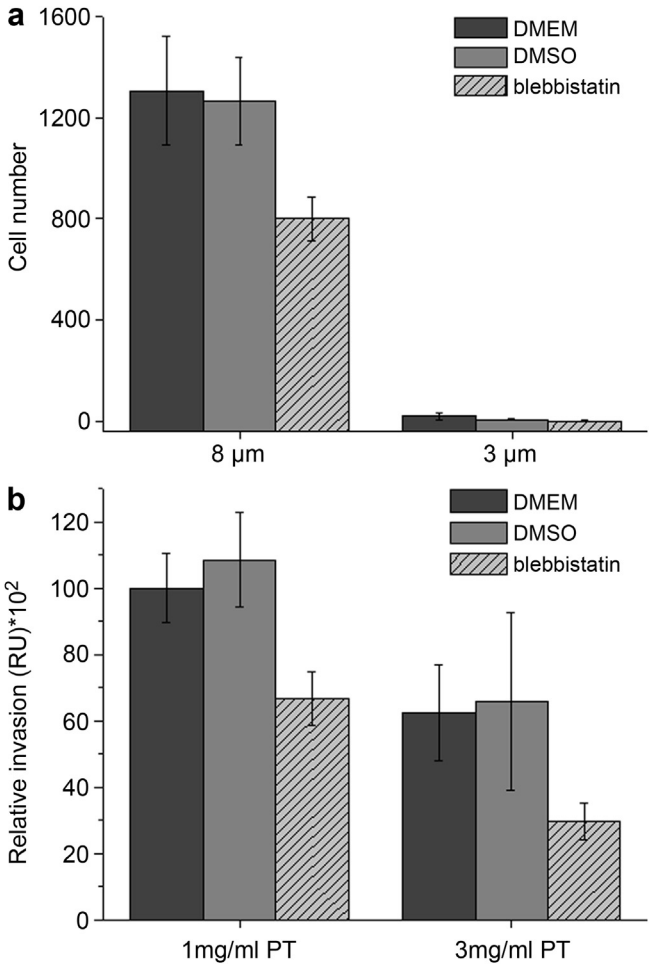

Fig. 3. Role of myosin-driven cell contractility in MDA-MB-231 invasion. (*a*) Transmigration of MDA-MB-231 cells in Transwell assays with (shaded) and without (solid) blebbistatin-mediated myosin II inhibition. Graph shows average cell counts ± SD per field of view of cells migrated within 24 h through a membrane with 8 μm or 3 μm pores. For quantification 20 images were taken from each sample and conditions were tested in at least duplicate. (*b*) MTS invasion in low (1.0 mg/ml) and high (3.0 mg/ml) density collagen gels under blebbistatin-mediated myosin II inhibition. $n = 4–6$ for every condition.

MDA-MB-231 MTSs, which efficiently invaded all tested collagen systems, failed to invade the highly compliant BME matrices to a comparable degree at any chosen concentration (Fig. 4). Placing the spheroids atop a BME matrix was not sufficient to rescue the invasive behavior, although the cells do not experience any steric hindrance in this pseudo-3D setting (Fig. 4a). Thus, the dramatic reduction of tumor cell invasiveness in these non-fibrillar matrices is not due to the elastic properties of the matrix nor is it exclusively caused by the physical constraints experienced by the cells. Beside the strongly reduced invasion distance, the morphology of the invading front was greatly altered in BME in comparison to fibrillar collagen matrices in both pseudo-3D and true 3D scenarios. Both atop and within BME matrices, the hallmarks of individual mesenchymal migration were lost, and the tumor spheroid adopted a collective mode of invasion accompanied by reduced cell polarity at the invading front (Fig. 4a).

To elucidate the molecular underpinnings of the differences in invasion mode and efficiency in collagen and BME, establishment of cell polarity and protrusions indicative of migratory behavior was assessed for individual cells within and atop fibrillar, non-fibrillar, and composite matrices. Cells were stained for actin

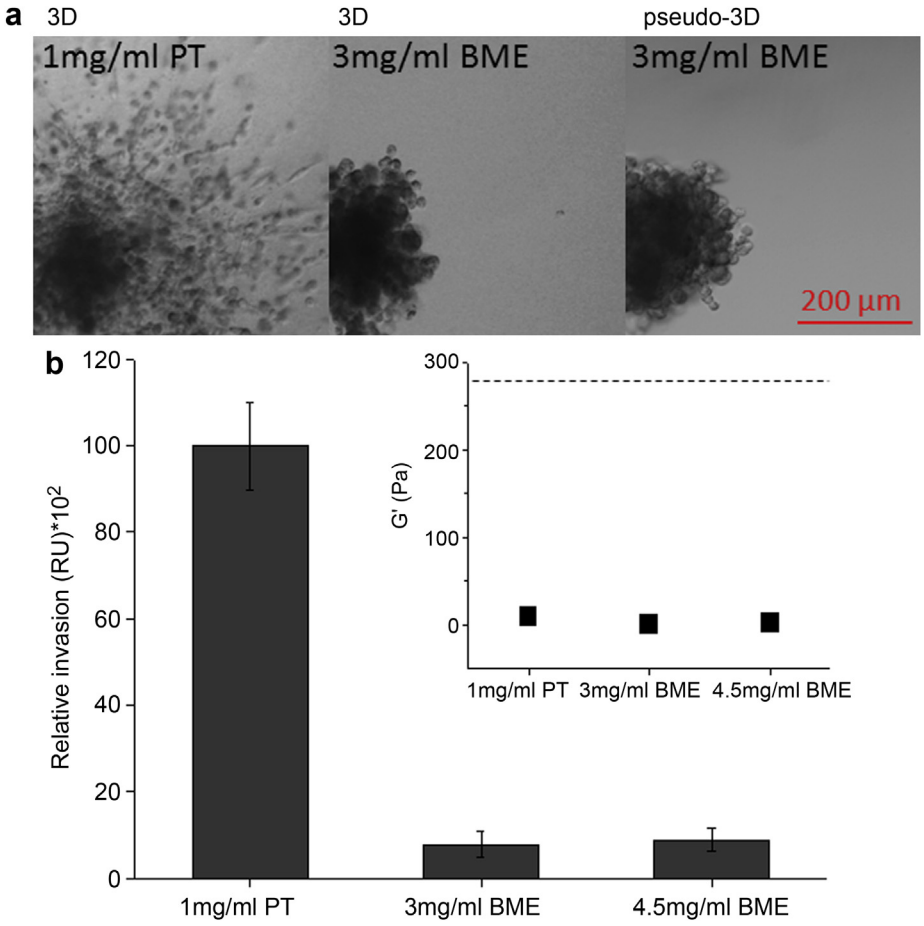

Fig. 4. MTS invasion in non-fibrillar environments. (*a*) Representative transmitted light images of spheroids after 24 h invasion (left) in 1.0 mg/ml collagen, (middle) in 3.0 mg/ml BME, and (right) on 3.0 mg/ml BME. Scale bar = 200 μm. A representative portion of each spheroid is shown to allow observation of full invasive distance. (*b*) Quantification of MTS invasion in the non-fibrillar BME compared to invasion in fibrillar collagen matrix. $n \geq 5$ for each condition. Inset: Storage moduli (G′) of 1.0 mg/ml PT collagen, 3.0 mg/ml BME, and 4.5 mg/ml BME; dotted line indicates the storage modulus of 4.0 mg/ml PT collagen. For these measurements, all sample chambers were pre-coated with the matrix employed.

cytoskeleton and categorized into polarized and non-polarized sub-populations by morphology and actin distribution at the cell periphery, with round cells lacking heterogeneous actin accumulation regarded as non-polarized (Fig. 5 and Supplementary Fig. 1). Cell protrusions were categorized as actin-polymerization-based (filopodia) or actomyosin contractility-based (blebs), and the occurrence of such protrusions in the polarized and non-polarized cell sub-population was determined. The population of polarized cells, which was predominant for cells both in and atop collagen matrices, was fully lost in the non-fibrillar BME environment regardless of whether the cells were within or atop the matrix (Fig. 5b). The establishment of either type of cell protrusions was reduced by 90% in the non-fibrillar matrix. The loss of stable cell protrusions occurred also for cells atop the non-fibrillar gel, even though steric constraints for the cells were absent in this scenario (Fig. 5c).

3.3. *Effect of fibrillar collagen in establishing a migratory phenotype*

The effects of the introduction of fibrillar collagen into the non-fibrillar BME matrix on cell polarity and protrusion formation were next assessed. To this end cells were implanted in composite matrices consisting of collagen I and varying concentrations of BME. One type of composite matrix comprised 1.0 mg/ml PT collagen and 3.0 mg/ml BME (1PT + 3BME). This composite is expected to have the same steric constraints present in the 3.0 mg/ml BME matrix plus a fibrillar matrix of PT collagen. Confocal imaging confirmed that collagen network architecture was similar in the presence and absence of BME (data not shown). The average storage moduli of the 1PT + 3BME gels was 22 Pa, somewhat higher than that of the corresponding non-composite gels but more than an order of magnitude lower than the stiffest gels used in this study (Supplementary Table 1). A second type of composite matrix composed of 1.0 mg/ml PT collagen and 1.0 mg/ml BME (1PT + 1BME) was also investigated. BME at 1.0 mg/ml forms a very weak gel (G′ = 0.13 Pa) incapable of supporting a spheroid. The composite matrix had a storage modulus quite similar to that of PT collagen alone. The BME in this matrix was thus liquid-like and expected to have very limited effect on the network architecture of the gel.

The introduction of collagen fibers indeed re-established polarity in cells on and in BME containing gels (Fig. 5b). For cells within composite matrices, the ratio of polarized to non-polarized cells correlated with the storage modulus of the matrix, which depended on whether the BME was in the liquid-like (1PT + 1BME) or fully gelled (1PT + 3BME) state. A similar trend was observed for establishment of cell protrusions, with the proportion of filopodia to blebs decreasing with increasing BME concentration in the 3D scenario. The polarization and formation of cell protrusions of cells atop composite matrices were not influenced by the variations in compliancy and gelation state of the BME component, as long as fibrillar collagen was present.

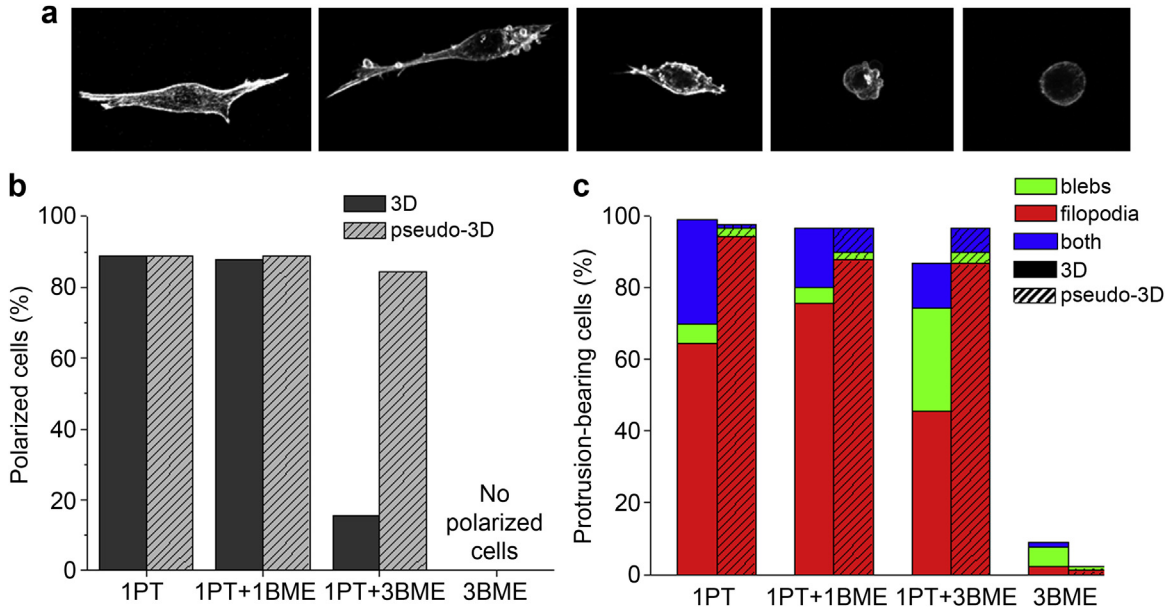

Fig. 5. Cell polarity and cell protrusions in various 3D environments. (*a*) Representative confocal fluorescence maximum projections of phalloidin-stained MDA-MB-231 cells embedded in 3D matrices depicting the range of cell types observed. Left to right images depict a polarized cell with filopodia, two polarized cells with filopodia and blebs, an unpolarized cell with blebs, and an unpolarized cell lacking protrusions. Z-stacks from two phalloidin-stained cells depicting both the cell and surrounding collagen are shown in Supplementary Fig. 1. (*b*) Percentage of polarized MDA-MB-231 cells in various 3D (solid) and pseudo-3D (shaded) environments. $n = 90$ with data pooled from 2 independent experiments. (*c*) Protrusion classes in various 3D (solid) and pseudo-3D (shaded) environments. $n = 90$ with data pooled from 2 independent experiments.

3.4. Invasion efficiency in composite matrices containing fibrillar collagen

Next, we analyzed whether the re-establishment of cell polarity and cell protrusions through the addition of fibrillar collagen was sufficient to re-establish MTS invasion in pseudo-3D and true 3D composite matrices. In the pseudo-3D setting, the introduction of collagen fibers was sufficient to fully rescue the invasive behavior of the MTSs regardless of the collagen:BME ratio. In the pseudo-3D composite matrices, invasive distance, morphology of the emigrating cells, and individual mode of migration were all comparable to those observed in 1.0 mg/ml PT collagen gels. In contrast, in a true 3D setting, invasion efficiency varied depending on the collagen:BME ratio (Fig. 6). Although invasion in the high content BME composite matrix was significantly less than in a 1.0 mg/ml collagen I lattice, it was increased by a factor of three relative to that in the pure BME matrix of the same BME concentration. Importantly, the introduction of collagen fibers not only strongly increased invasive distance but also reconstituted the predominantly individual mesenchymal mode of migration observed in single component fibrillar matrices (Fig. 6a). Interestingly, the 3D invasion observed over 24 h correlated with the degree of collagen fiber reorganization that took place as early as 2 h after spheroid implantation. In 1.0 mg/ml PT collagen, the most efficiently invaded environment studied, extensive collagen reorganization around the spheroid periphery was evident. Conversely, in composite matrices with high BME content, there was only limited early matrix reorganization and modest invasion (Fig. 6b).

4. Discussion

In this study, the contributions of substrate stiffness, pore size, and especially fibrillar versus non-fibrillar network architecture to the efficiency and mode of tumor cell invasion were investigated.

Invasion of tumor spheroids placed atop (pseudo-3D) fibrillar matrices showed no clear correlation with collagen concentration while invasion within such matrices was limited at higher collagen concentrations, apparently by the steric constraints experienced by cells (Fig. 1c). This is in accordance with other works on the impact of physical limitations to 3D invasion [28,37,38]. To more clearly differentiate the impact of steric (pore size) and mechanical (stiffness) matrix properties from the bulk substrate concentration, a tunable collagen system that allows pore size and compliancy to be modulated independent of collagen concentration was employed [37]. Analysis of invasion within this tunable collagen system demonstrated that in a true 3D environment the invasion-limiting impact of small pore sizes dominates over possible advantageous effects of higher stiffness or increased ligand availability present in high density matrices, an effect that cannot be assessed in 2D or pseudo-3D settings. While pore size smaller than nuclear size increasingly limited invasive distance, with very similar sensitivity to pore size seen across different cancer cell types [37,38], overall the invasive behavior of MDA-MB-231 spheroids in collagen gels was robust: only intermediate quantitative changes ($\approx$2 fold) in invasive distance were evident and no obvious changes in migratory phenotype over a broad range of pore size, fiber dimensions, and substrate stiffness were observed (Fig. 2).

Relatively effective invasion was seen even in cells invading high density gels with protease inhibition. Matrix metalloproteinases (MMPs) have been found to be deregulated and have been proposed to play a role in the progression of multiple cancers including breast cancer [39–41]. Recent *in vitro* work suggested that inhibiting MMP activity in telopeptide-bearing AS collagen may abolish invasion while doing so in telopeptide-deficient PT collagen may force cells to adopt an amoeboid mode of invasion [38]. In this work, invasive distance of spheroids in collagen gels with (AS) or without (PT) intact telopeptides was comparable at both low (1.0 mg/ml) and high (4.0 mg/ml) collagen concentration (Fig. 1d). Pharmacological inhibition of MMPs reproducibly reduced invasive distance in AS and PT collagen matrices by similar amounts and did not effect an obvious switch in migratory phenotype in any matrix type. The observation that protease inhibition limited invasion

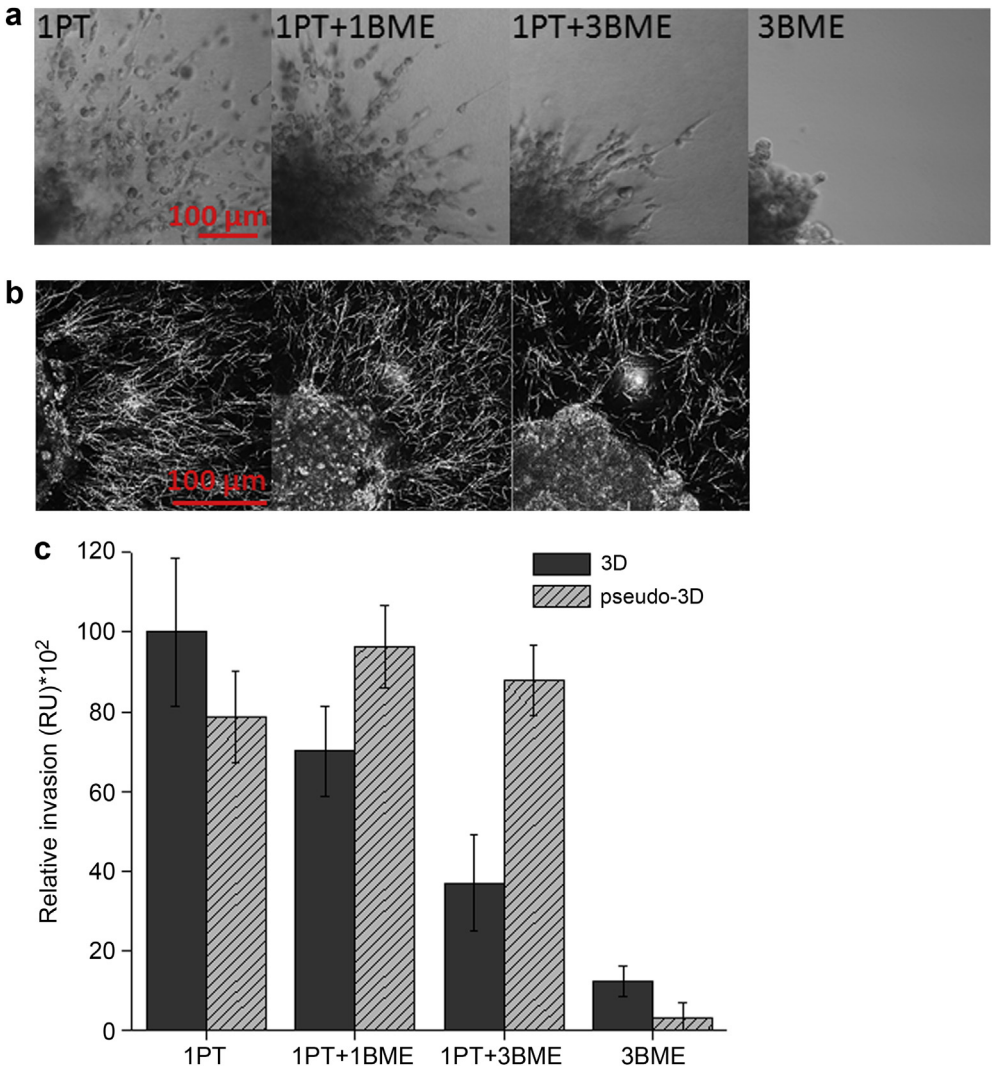

Fig. 6. MTS invasion efficiency in and on BME matrices increases with introduction of fibrillar collagen. (*a*) Representative transmitted light images of MTSs after 24 h invasion in, from left to right, 1.0 mg/ml collagen (1PT), 1.0 mg/ml collagen+1.0 mg/ml BME (1PT + 1BME), 1.0 mg/ml collagen + 3.0 mg/ml BME (1PT + 3BME), and 3.0 mg/ml BME (3BME). Scale bar = 100 μm. A representative portion of each spheroid is shown to allow observation of full invasive distance. (*b*) Representative CRM images of a representative portion of MTSs 2 h after implantation in, from left to right, 1PT, 1PT + BME, and 1PT + 3BME. Scale bar = 100 μm. Spheroids in (b) are not the same ones shown in (a). (*c*) MTS invasion in (solid) and on (shaded) various fibrillar, non-fibrillar, and composite environments. $n \geq 9$ for each 3D condition, $n \geq 4$ for each pseudo-3D condition. For these measurements, all sample chambers were pre-coated with the matrix employed.

similarly in all collagen gels suggests roles for these proteases beyond that of collagen degradation [42].

Though pore size was found to be the strongest determinant of invasion efficiency in 3D fibrillar matrices (Fig. 2), the effect was less stark than would be expected from results seen in trans-migration assays with and without blebbistatin-mediated inhibition of cell contractility (Fig. 3). This may be related to the deformability of the collagen system and suggested that the presence of collagen fibers may assist cell migration through small pores. To test this hypothesis, cell invasion was measured in non-fibrillar (BME) and mixed fibrillar/non-fibrillar environments (collagen/BME composites) of similar elasticity.

MDA-MB-231 spheroids failed to efficiently invade 3D BME matrices at any concentration (2.5–9 mg/ml BME). The stiffness and pore size of BME matrices are correlated with its protein content, and while stiffness of employed BME matrices was comparable to low density collagen gels, average pore size in all cases is expected to be <1 μm [34–36]. While subcellular pore size in fibrillar collagen networks induced only a moderate quantitative change in MTS invasion (40–50%), the non-fibrillar environment led to a 90% reduction in invasive distance. Moreover, a qualitative switch of invasive mode from individual migration with a robust population of cells with typical mesenchymal phenotype to collective motion with few extended, polarized cells was seen (Fig. 4), consistent with previous measurements of primary human breast carcinoma behavior [43]. This dramatic loss of invasive behavior cannot be explained by lack of appropriate surface receptors. MDA-MB-231 cells express clearly detectable amounts of α2β1 integrin (data not shown) [44], which apart from being a collagen I receptor can also bind laminin and collagen IV, the primary components of BME [45]. Moreover, high expression of α3β1 integrin, one of the main laminin-binding integrins, has been reported for MDA-MB-231 cells [44,46]. The failure to invade BME matrices was also not due to stiffness of the matrix, as BME gel storage moduli were comparable to those of collagen gels supporting significant invasion (Fig. 4, Supplementary Table 1, Supplementary Fig. 2). Interestingly, the invasive behavior was not reconstituted by placing the spheroids atop thick BME matrices, which offer the cells the same

biochemical substrate without the physical constraints of the 3D environment. Thus, the failure of spheroids to invade the non-fibrillar BME matrix is not due primarily to physical constraints of subcellular pores or the absence of suitable cell surface receptors. We suggest instead that it is due to the lack of suitable spatial organization of adhesion ligands.

Analysis of cell morphology and cell protrusions of cells implanted in and atop different types of 3D matrices support the view that organization of ligands is critical to establishing a migratory phenotype not only in but also on adhesive substrates. This analysis revealed that cell polarization and the formation of stable cell protrusions – two hallmarks of migratory behavior – were heavily compromised or fully lost in non-fibrillar matrices (Fig. 5). As with invasion, the establishment of cell polarity and the formation of protrusions were compromised not primarily by the steric constraints of the sheet-like BME matrix, as cell polarity was not rescued through plating cells atop the matrix. Rather, both cell polarity and protrusions were re-established upon the introduction of fibrillar collagen into the BME matrix (Fig. 5b). These results suggest that cell polarity and protrusions require the physical cues provided by the fibrillar substrate regardless of whether the cell is confronted with additional physical challenges. In true 3D environments, where steric constraints may be present, fibrillar architecture is necessary but not sufficient to fully reconstitute characteristics of 3D invasion seen in permissive fibrillar collagen environments. A strong reduction of the polarized cell population was seen with increasing BME content in collagen/BME composite matrices (Fig. 5b). While the same increase in BME concentration resulted in only a minimally reduced percentage of protrusion-bearing cells, a clear shift from actin-polymerization-based protrusions (filopodia) to pressure-driven blebs, spherical protrusions that are associated with an alternate mode of cell motility [47], was evident. Taken together, these findings suggest that steric impairment of the environment counteracts and limits actin-polymerization-dependent processes employed in migratory behavior. These results demonstrate that efficiency of 3D invasion strongly correlates with cell polarization and type of cell protrusions on a single cell level, features that have previously been suggested to be indicators of metastatic potential [48,49].

Cell polarization and adoption of a mesenchymal migratory phenotype also correlated with the degree cells reorganized the collagen matrix preceding invasion (Fig. 6). In general, matrices in which rapid collagen rearrangement around the spheroid front occurred also supported efficient spheroid invasion. Interestingly, the collagen conditions that allowed for efficient reorganization did not fully coincide with the conditions in which significant matrix contraction through individual cells was observed (Supplementary Figs. 2 and 3). While matrix contraction strongly correlated with the viscoelastic properties of the matrix and took place only in fibrillar matrices with $G' < 10$ Pa, efficient spheroid reorganization and invasion was observed not only in those gels but also in the stiffest collagen gels investigated, those composed of fiber bundles (Fig. 2a, Supplementary Fig. 3). Among all gels, including those supportive of invasion but not contracted in contraction assays, invasive distance correlated with degree of reorganization in the immediate environment of the spheroid (Fig. 6). It remains to be clarified whether the ability for spheroids to re-organize collagen and invade a matrix that dispersed cells fail to contract is due to higher expression of mechanotransductory components by cells grown in aggregate, more efficient compartmentalization of these molecules, and/or the geometry of the spheroid front that encourages cell polarization through presentation of ECM ligands anisotropically around leading invasive cells. No matter the origin of these effects, these results – as well as the demonstration of the importance of the full 3D network architecture on invasion efficiency – underline the utility of multicellular aggregates as *in vitro* models for studying key events of the metastatic process.

5. Conclusions

This study elucidates the crucial role of the biophysical cues provided by fibrillar collagen for cancer cell invasion in sterically challenging environments. We demonstrate the dominant role of pore size over stiffness for invasion efficiency in fibrillar environments and the indispensable role of fibrillar substrate for invasion in composite matrices. The presence of collagen fibers assists tumor cells in invading otherwise non-favorable environments by inducing cell polarization and formation of stable cell protrusions. This study demonstrates that the presence of fibrillar substrate is sufficient to allow breast cancer cells to establish a migratory phenotype and invade environments that otherwise inhibit migration through steric constraints. Finally, we suggest that the 3D composite collagen/BME matrices introduced in this study may be particularly suitable systems for assessment of cell behavior as they test not only the effects of physical cues provided by fibrillar substrates and contributions of force generation but also can be tuned to probe cell ability to invoke alternate migratory phenotypes necessary in dense non-fibrillar environments.

Acknowledgments

This work was supported by the National Science Foundation and the National Institutes of Health via PESO 1227297.

Appendix A. Supplementary data

Supplementary data related to this article can be found at http://dx.doi.org/10.1016/j.biomaterials.2014.04.086.

References

[1] Kothapalli D, Liu SL, Bae YH, Monslow J, Xu T, Hawthorne EA, et al. Cardiovascular protection by ApoE and ApoE-HDL linked to suppression of ECM gene expression and arterial stiffening. Cell Rep 2012;2:1259–71.
[2] Georges PC, Hui JJ, Gombos Z, McCormick ME, Wang AY, Uemura M, et al. Increased stiffness of the rat liver precedes matrix deposition: implications for fibrosis. Am J Physiol Gastrointest Liver Physiol 2007;293:G1147–54.
[3] Cox TR, Erler JT. Remodeling and homeostasis of the extracellular matrix: implications for fibrotic diseases and cancer. Dis Model Mech 2011;4:165–78.
[4] Perepelyuk M, Terajima M, Wang AY, Georges PC, Janmey PA, Yamauchi M, et al. Hepatic stellate cells and portal fibroblasts are the major cellular sources of collagens and lysyl oxidases in normal liver and early after injury. Am J Physiol Gastrointest Liver Physiol 2013;304:G605–14.
[5] Paszek MJ, Zahir N, Johnson KR, Lakins JN, Rozenberg GI, Gefen A, et al. Tensional homeostasis and the malignant phenotype. Cancer Cell 2005;8:241–54.
[6] Levental KR, Yu H, Kass L, Lakins JN, Egeblad M, Erler JT, et al. Matrix crosslinking forces tumor progression by enhancing integrin signaling. Cell 2009;139:891–906.
[7] Kumar S, Weaver VM. Mechanics, malignancy, and metastasis: the force journey of a tumor cell. Cancer Metastasis Rev 2009;28:113–27.
[8] Lu P, Weaver VM, Werb Z. The extracellular matrix: a dynamic niche in cancer progression. J Cell Biol 2012;196:395–406.
[9] Cil T, Fishell E, Hanna W, Sun P, Rawlinson E, Narod SA, et al. Mammographic density and the risk of breast cancer recurrence after breast-conserving surgery. Cancer 2009;115:5780–7.
[10] Boyd NF, Martin LJ, Yaffe MJ, Minkin S. Mammographic density and breast cancer risk: current understanding and future prospects. Breast Cancer Res 2011;13:223.
[11] Alowami S, Troup S, Al-Haddad S, Kirkpatrick I, Watson PH. Mammographic density is related to stroma and stromal proteoglycan expression. Breast Cancer Res 2003;5:R129–35.
[12] Guo YP, Martin LJ, Hanna W, Banerjee D, Miller N, Fishell E, et al. Growth factors and stromal matrix proteins associated with mammographic densities. Cancer Epidemiol Biomarkers Prev 2001;10:243–8.
[13] Deak SB, Glaug MR, Pierce RA, Bancila E, Amenta P, Mackenzie JW, et al. Desmoplasia in benign and malignant breast disease is characterized by

alterations in level of mRNAs coding for types I and III procollagen. Matrix 1991;11:252–8.
[14] Kauppila S, Stenback F, Risteli J, Jukkola A, Risteli L. Aberrant type I and type III collagen gene expression in human breast cancer in vivo. J Pathol 1998;186:262–8.
[15] Bergamaschi A, Tagliabue E, Sorlie T, Naume B, Triulzi T, Orlandi R, et al. Extracellular matrix signature identifies breast cancer subgroups with different clinical outcome. J Pathol 2008;214:357–67.
[16] Krouskop TA, Wheeler TM, Kallel F, Garra BS, Hall T. Elastic moduli of breast and prostate tissues under compression. Ultrason Imaging 1998;20:260–74.
[17] Chang JM, Park IA, Lee SH, Kim WH, Bae MS, Koo HR, et al. Stiffness of tumours measured by shear-wave elastography correlated with subtypes of breast cancer. Eur Radiol 2013;23:2450–8.
[18] Lo CM, Wang HB, Dembo M, Wang YL. Cell movement is guided by the rigidity of the substrate. Biophys J 2000;79:144–52.
[19] Engler AJ, Sen S, Sweeney HL, Discher DE. Matrix elasticity directs stem cell lineage specification. Cell 2006;126:677–89.
[20] Zaman MH, Trapani LM, Sieminski AL, Mackellar D, Gong H, Kamm RD, et al. Migration of tumor cells in 3D matrices is governed by matrix stiffness along with cell-matrix adhesion and proteolysis. Proc Natl Acad Sci U S A 2006;103:10889–94.
[21] Ulrich TA, Lee TG, Shon HK, Moon DW, Kumar S. Microscale mechanisms of agarose-induced disruption of collagen remodeling. Biomaterials 2011;32:5633–42.
[22] Pathak A, Kumar S. Independent regulation of tumor cell migration by matrix stiffness and confinement. Proc Natl Acad Sci U S A 2012;109:10334–9.
[23] Ehrbar M, Sala A, Lienemann P, Ranga A, Mosiewicz K, Bittermann A, et al. Elucidating the role of matrix stiffness in 3D cell migration and remodeling. Biophys J 2011;100:284–93.
[24] Beck JN, Singh A, Rothenberg AR, Elisseeff JH, Ewald AJ. The independent roles of mechanical, structural and adhesion characteristics of 3D hydrogels on the regulation of cancer invasion and dissemination. Biomaterials 2013;34:9486–95.
[25] Provenzano PP, Eliceiri KW, Campbell JM, Inman DR, White JG, Keely PJ. Collagen reorganization at the tumor-stromal interface facilitates local invasion. BMC Med 2006;4:38.
[26] Conklin MW, Eickhoff JC, Riching KM, Pehlke CA, Eliceiri KW, Provenzano PP, et al. Aligned collagen is a prognostic signature for survival in human breast carcinoma. Am J Pathol 2011;178:1221–32.
[27] Wolf K, Mazo I, Leung H, Engelke K, von Andrian UH, Deryugina EI, et al. Compensation mechanism in tumor cell migration: mesenchymal-amoeboid transition after blocking of pericellular proteolysis. J Cell Biol 2003;160:267–77.
[28] Kaufman LJ, Brangwynne CP, Kasza KE, Filippidi E, Gordon VD, Deisboeck TS, et al. Glioma expansion in collagen I matrices: analyzing collagen concentration-dependent growth and motility patterns. Biophys J 2005;89:635–50.
[29] Raub CB, Suresh V, Krasieva T, Lyubovitsky J, Mih JD, Putnam AJ, et al. Noninvasive assessment of collagen gel microstructure and mechanics using multiphoton microscopy. Biophys J 2007;92:2212–22.
[30] Yang YL, Leone LM, Kaufman LJ. Elastic moduli of collagen gels can be predicted from two-dimensional confocal microscopy. Biophys J 2009;97:2051–60.
[31] Fu Y, Chin LK, Bourouina T, Liu AQ, VanDongen AM. Nuclear deformation during breast cancer cell transmigration. Lab Chip 2012;12:3774–8.
[32] Straight AF, Cheung A, Limouze J, Chen I, Westwood NJ, Sellers JR, et al. Dissecting temporal and spatial control of cytokinesis with a myosin II inhibitor. Science 2003;299:1743–7.
[33] Kovacs M, Toth J, Hetenyi C, Malnasi-Csizmadia A, Sellers JR. Mechanism of blebbistatin inhibition of myosin II. J Biol Chem 2004;279:35557–63.
[34] Yurchenco PD, Ruben GC. Basement-membrane structure in situ – evidence for lateral associations in the type-IV collagen network. J Cell Biol 1987;105:2559–68.
[35] Abrams GA, Goodman SL, Nealey PF, Franco M, Murphy CJ. Nanoscale topography of the basement membrane underlying the corneal epithelium of the rhesus macaque. Cell Tissue Res 2000;299:39–46.
[36] Kalluri R. Basement membranes: structure, assembly and role in tumour angiogenesis. Nat Rev Cancer 2003;3:422–33.
[37] Yang YL, Motte S, Kaufman LJ. Pore size variable type I collagen gels and their interaction with glioma cells. Biomaterials 2010;31:5678–88.
[38] Wolf K, Te Lindert M, Krause M, Alexander S, Te Riet J, Willis AL, et al. Physical limits of cell migration: control by ECM space and nuclear deformation and tuning by proteolysis and traction force. J Cell Biol 2013;201:1069–84.
[39] Murray GI, Duncan ME, O'Neil P, Melvin WT, Fothergill JE. Matrix metalloproteinase-1 is associated with poor prognosis in colorectal cancer. Nat Med 1996;2:461–2.
[40] Nakopoulou L, Giannopoulou I, Gakiopoulou H, Liapis H, Tzonou A, Davaris PS. Matrix metalloproteinase-1 and -3 in breast cancer: correlation with progesterone receptors and other clinicopathologic features. Hum Pathol 1999;30:436–42.
[41] McGowan PM, Duffy MJ. Matrix metalloproteinase expression and outcome in patients with breast cancer: analysis of a published database. Ann Oncol 2008;19:1566–72.
[42] Butler GS, Overall CM. Updated biological roles for matrix metalloproteinases and new "intracellular" substrates revealed by degradomics. Biochemistry 2009;48:10830–45.
[43] Nguyen-Ngoc KV, Cheung KJ, Brenot A, Shamir ER, Gray RS, Hines WC, et al. ECM microenvironment regulates collective migration and local dissemination in normal and malignant mammary epithelium. Proc Natl Acad Sci U S A 2012;109:E2595–604.
[44] Mierke CT, Frey B, Fellner M, Herrmann M, Fabry B. Integrin alpha5beta1 facilitates cancer cell invasion through enhanced contractile forces. J Cell Sci 2011;124:369–83.
[45] Plow EF, Haas TA, Zhang L, Loftus J, Smith JW. Ligand binding to integrins. J Biol Chem 2000;275:21785–8.
[46] Nishiuchi R, Takagi J, Hayashi M, Ido H, Yagi Y, Sanzen N, et al. Ligand-binding specificities of laminin-binding integrins: a comprehensive survey of laminin-integrin interactions using recombinant alpha3beta1, alpha6beta1, alpha7beta1 and alpha6beta4 integrins. Matrix Biol 2006;25:189–97.
[47] Charras G, Paluch E. Blebs lead the way: how to migrate without lamellipodia. Nat Rev Mol Cell Biol 2008;9:730–6.
[48] Meyer AS, Hughes-Alford SK, Kay JE, Castillo A, Wells A, Gertler FB, et al. 2D protrusion but not motility predicts growth factor-induced cancer cell migration in 3D collagen. J Cell Biol 2012;197:721–9.
[49] Klemke RL. Trespassing cancer cells: 'fingerprinting' invasive protrusions reveals metastatic culprits. Curr Opin Cell Biol 2012;24:662–9.